JOURNAL OF NEUROTRAUMA
Volume 20, Number 5, 2003

Morphological Characterization of Photochemical Graded Spinal Cord Injury in the Rat

ENRIQUE VERDÚ,[1] GUILLERMO GARCÍA-ALÍAS,[1] JOAQUIM FORÉS,[1,2] JOSÉ M. VELA,[1] JORDI CUADRAS,[1] RUBEN LÓPEZ-VALES,[1] and XAVIER NAVARRO[1]

ABSTRACT

This study characterizes the histological and immunohistochemical changes in the adult rat spinal cord following photochemically induced spinal cord lesions. The spinal cord was exposed by laminectomy (T12–L1 vertebrae) and bathed with 1.5% rose bengal solution for 10 min. The excess dye was removed by saline rinse and the spinal cord was irradiated with "cold" light for 0, 1, 2.5, 5, and 10 min in different groups of rats. After 15 days a graded loss of spinal tissue was observed according to photoinduction times. Animals irradiated for 1 min showed spinal cavities involving the dorsal funiculi. The cavity became progressively larger, involving dorsal horns in animals irradiated for 2.5 min, together with the dorsolateral funiculi in animals irradiated for 5 min and the ventrolateral funiculi in those irradiated for 10 min, with loss of gray matter in these three groups. Changes in GFAP-, CGRP-, proteoglycan- and calbindin-immunoreactivity were observed in all lesioned groups when compared with control spinal cords. Hypertrophied and heavily GFAP- and proteoglycan-stained astrocytes were seen in irradiated spinal cords. Reactive microglial cells were also found. Both astroglial and microglial reactions paralleled the severity of the spinal cord lesion. A significant loss of CGRP-immunoreactive somas was seen in animals irradiated for 10 min, whereas the wider distribution of calbindin-positive neurons was found in lesioned rats. In spinal cord sections from animals illuminated for 5 min and perfused 60 min postillumination, light and electron microscopy showed cytotoxic edema with astrocytic swelling, red blood cell extravasation, and myelin degradation.

Key words: glial response; immunohistochemistry; photochemical injury, rose bengal; spinal cord

INTRODUCTION

SEVERAL EXPERIMENTAL MODELS have been used to produce spinal cord injury, including mechanical impact, compression of the cord with an inflatable epidural balloon, crushing the cord with forceps or aneurysm clip and photochemical lesions using rose bengal (tetrachlorotetraiodofluorescein) or erythrosin B (disodium-tetraiodofluorescein) (Anderson and Stokes, 1992; von Euler et al., 1997; Watson et al., 1993; Wrathall, 1992). The photochemical-induced injury has raised interest because it has similarities with traumatic spinal cord injuries in humans and it can be graded in severity. Using light and electron microscopy, previous reports detailed the mor-

[1]Department of Cell Biology, Physiology and Immunology, Universitat Autònoma de Barcelona, Bellaterra.
[2]Hand Unit, Hospital Clínic i Provincial, University of Barcelona, Barcelona, Spain.

phological consequences of photochemical lesions induced in the spinal cord after intravascular injection of a bolus of rose bengal (10–40 mg/kg) and subsequent cord irradiation with a laser beam (Bunge et al., 1994; Cameron et al., 1990; Prado et al., 1987; Van Reempts and Borgers, 1994; Watson et al., 1993). A necrotic cavity was observed 48 h after irradiation in the epicenter of the exposed spinal cord segments, involving the dorsal funiculus, dorsal horns and dorsolateral funiculi. The number of macrophages increased in the lesion cavity and several layers of flattened astrocytes appeared bordering the lesion. Adjacent to the lesion cavity, axons were swollen and only partly encased in myelin and in the peripheral regions remyelination by both oligodendrocytes and Schwann cells was observed by 14 days post-lesion. By 8 weeks, the lesion cavity decreased in size and contained scattered macrophages, Schwann cell–myelinated axons and blood vessels.

The expression of several markers has been shown to change in the central nervous system (CNS) after peripheral or central injuries. Reactive astrocytes upregulate proteoglycan and glial fibrillary acidic protein (GFAP) expression and immunoreactivity following mechanical (Baldwin et al., 1998; Farooque et al., 1995; Lemons et al., 1999) and photochemical (Verdú et al., 2001; von Euler et al., 1997) spinal cord injuries. The increased expression of GFAP is closely related to the severity of the spinal cord lesion (Farooque et al., 1995). Microglial reaction is also a common feature in CNS lesions and there is a close correspondence between the degree of microglial reaction and the degree of tissue involvement (Kreutzberg, 1996). In the spinal cord, microglial reaction has been described in a variety of pathological conditions, including spinal cord (Krenz and Weaver, 2000) and sciatic nerve (Köbbert and Thanos, 2000) transection, and photochemically induced cord lesion (Koshinaga and Whittemore, 1995). Regarding neurons, it is well known that a number of cells degenerate following spinal cord injury (Beattie et al., 2000), but less is known about the neuronal expression of neuropeptides having a role in the adaptive response to the injury, survival, growth and regeneration. Calcitonin gene–related peptide (CGRP) is a developmentally regulated trophic neuropeptide whose expression after CNS injury in the adult has been related to axonal growth and motoneuron survival (Blesch and Tuszynski, 2001). CGRP immunoreactivity in spinal motoneurons increases after peripheral nerve injury (Borke et al., 1993; Calderó et al., 1992) but it is down-regulated in motoneurons below a spinal cord transection (Arvidsson et al., 1989; Marlier et al., 1990; Melinek et al., 1994). Calbindin-D28k plays also an important role in the regulation of calcium homeostasis, buffering abnormal calcium concentrations that may be cytotoxic (Nicotera et al., 1992), and neurons in lamina I and II exhibit intense calbindin-D28k immunoreactivity after dorsal root ganglionectomy (Ren and Ruda, 1994).

The expression of morpho-functional glial and neuronal markers has not been studied in detail after photochemical injuries. Astrocyte and microglia reactivity was previously analyzed only shortly after (2.5–10 min) photochemical irradiation (Koshinaga and Whittermore, 1995; Koshinaga et al., 1993; von Euler et al., 1997). In this paper we present histological and immunohistochemical evaluation of photochemical injury of the rat spinal cord induced by a modified method using rose bengal and "cold" light irradiation. We first studied how the dye (rose bengal) applied topically infiltrates the cord parenchyma, and after illumination affects the spinal cord. In a second part, we have analyzed the effects of illumination time on the severity of spinal cord injury during 15 days postlesion. This time interval was chosen because previous studies indicated that the main morphological changes occur during the first 2–3 weeks postinjury (Bunge et al., 1994; Cameron et al., 1990; Koshinaga and Whittemore, 1995; von Euler et al., 1997). Different neuronal, astroglial and microglial markers were used. GFAP and proteoglycan are both selectively found in astrocytes (Bovolenta et al., 1997), lectin obtained from *Lycopersicon esculentum* (tomato) selectively binds to microglial cells (Acarin et al., 1994), calbindin D-28k protein is expressed by interneurons (Ren and Ruda, 1994) and CGRP is present in dorsal sensory nerve fibers and motoneurons (Gibson et al., 1984).

MATERIALS AND METHODS

Spinal Cord Injury

Female Sprague-Dawley rats (250–300 g) were anesthetized with sodium pentobarbital (50 mg/kg, i.p.), and the back of the animal was shaved and disinfected with povidone iodine. The animal was placed in a stereotactic frame, the skin and muscles were cut longitudinally and the spinal cord was exposed by a dorsal laminectomy at T12–L1 vertebrae. The dura was carefully cut to facilitate penetration of solutions. Bupivacaine solution (0.5%) was topically applied to minimize nociceptive input. Then, rose bengal (RB; 1.5% in saline, Sigma) was applied directly on the exposed spinal cord during 10 min. The excess dye was removed by a double saline rinse.

The lesion was induced by illuminating the exposed dorsal surface of the spinal cord by means of two optic fibers, with a diameter of 5 mm, positioned 10 mm on

top of the cord. The size of the illuminated dorsal surface was about 2 × 10 mm. The optic fibers were connected to a halogen lamp (Raypa, Barcelona, Spain) equipped with a 150-W Xenophot halogen bulb (EFP 64634 HLX, OSRAM, Germany). Using a digital lux tester (YF-1065, YUFING, Taiwan), we measured the irradiation power at the fiber outlet. The spinal cord was illuminated at a maximal light intensity of 120 kLux during different times (see below). The wavelength light of the halogen bulb is included in the visible spectrum (about 400–700 nm). To prevent damage by the calorific source of the halogen lamp, during the illumination time the spinal cord was bathed with saline solution. Finally, the wound was closed with 5-0 silk thread in the muscular plane and with small clips at the skin. During surgery, body temperature was maintained at 37 ± 0.5°C with a thermostated surgical blanket. The animals were kept in a warm environment until full recovery and were given amitriptyline (150 μg/mL) in the drinking water to prevent neuropathic pain (Navarro et al., 1994). The experimental procedures adhered to the recommendations of the European Union and the U.S. Department of Health for the care and use of laboratory animals and were approved by the Ethics Committee of our institution.

Rose Bengal Infiltration and Effects of Spinal Cord Illumination

The dye infiltration was studied in a group of 10 rats, which underwent a dorsal laminectomy and topical bathing of the spinal cord with RB solution for 10 min, as described above, but no illumination. Rats were transcardially perfused with 4% paraformaldehyde in phosphate-buffered saline solution (PBS, 0.1 M, pH 7.4). Spinal cord segments subjacent to T12–L1 vertebrae were removed, divided into two blocks, and postfixed with the same solution during 4 h at 4°C, then cryoprotected in PBS containing 30% sucrose. Cryotome transverse sections (100 μm thick) were mounted on gelatin-coated slides, and either directly viewed or dehydrated in ethanol, mounted with dextropropoxyphene (DPX, Fluka) and observed under light microscope.

Six rats were used for studying the early progress of the injury induced by RB illumination. After bathing the dorsal surface with the dye, the spinal cord was illuminated during 5 min as described above. At 5, 15, and 60 min post-illumination, two rats by time point were transcardially perfused with Karnovski solution (2% paraformaldehyde, 2.5% glutaraldehyde, 5% sacarose in 0.1 M cacodylate buffer solution at pH 7.4), and the spinal cord segments subjacent to T12-L1 vertebrae were removed and postfixed in the same solution. Samples were postfixed in OsO_4 (2%, 2h) at room temperature, dehydrated through ethanol series, stained with uranyl acetate (2.5%), and embedded in epon resin. Transverse semithin sections (1 μm thick) of the whole spinal cord were stained with toluidine blue and examined under light microscopy. Ultra-thin sections (70 nm) were viewed in an electron microscope (Hitachi H7000). Two intact rats were also perfused and the same spinal cord segments removed and embedded in epon resin.

Graded Spinal Cord Injury

After bathing with the RB solution, rats were illuminated during different times depending on the desired injury grade: 1 min (group RB1, $n = 5$), 2.5 min (group RB2.5, $n = 6$), 5 min (group RB5, $n = 10$), or 10 min (group RB10, $n = 5$). A group of five rats were bathed with RB but not illuminated (group RB0). In a control group, the spinal cord was bathed with saline solution alone and illuminated for 10 min (group SS10, $n = 5$). At 15 days, all rats were perfused and spinal cords removed and analyzed by histological and immunohistochemical techniques.

Immunohistochemical and Histochemical Methods

The animals were anesthetized and perfused transcardially with 4% paraformaldehyde in PBS. The spinal cords were removed, fixed in the same solution for 24 h and divided into several blocks identified as corresponding to T9–T10, T11, T12–L1, L2–L3, and L4–L6 spinal segments. Blocks were postfixed in Zamboni's fixative solution during 24 h, then cryoprotected in PBS containing 30% sucrose and stored at 4°C. Serial cryotome transverse sections 100 μm thick were washed free-floating in PBS with 0.3% Triton-X-100 (Fluka) and 1% normal goat serum (ICN Pharmaceuticals) for 1 h and incubated during 24 or 48 h at 4°C with rabbit antisera to GFAP (1:200, Chemicon), CGRP (1:1000, Amersham), and calbindin D-28k protein (CB; 1:1000, Chemicon), mouse antiserum to proteoglycan (3PE8; 1:400) and biotinylated tomato lectin (LEC; 1:100, Sigma). After washes, sections were incubated with secondary antiserum, donkey anti-rabbit or donkey anti-mouse Cy2- or Cy3-labeled immunoglobulin G (1:200, Jackson Immunoresearch) and Cy2-labeled avidin (1:200, Jackson Immunoresearch) overnight at 4°C. Following additional washes, sections were mounted on gelatin-coated slides, dehydrated in ethanol and mounted with DPX. As a specificity control, some spinal cord sections were incubated without primary antibody, and processed as described above. Samples were viewed under an Olympus BX-40 microscope equipped with epifluorescence using appropriate filters.

Low-power magnification (×10) images of spinal cord sections were taken with the aid of a digital camera

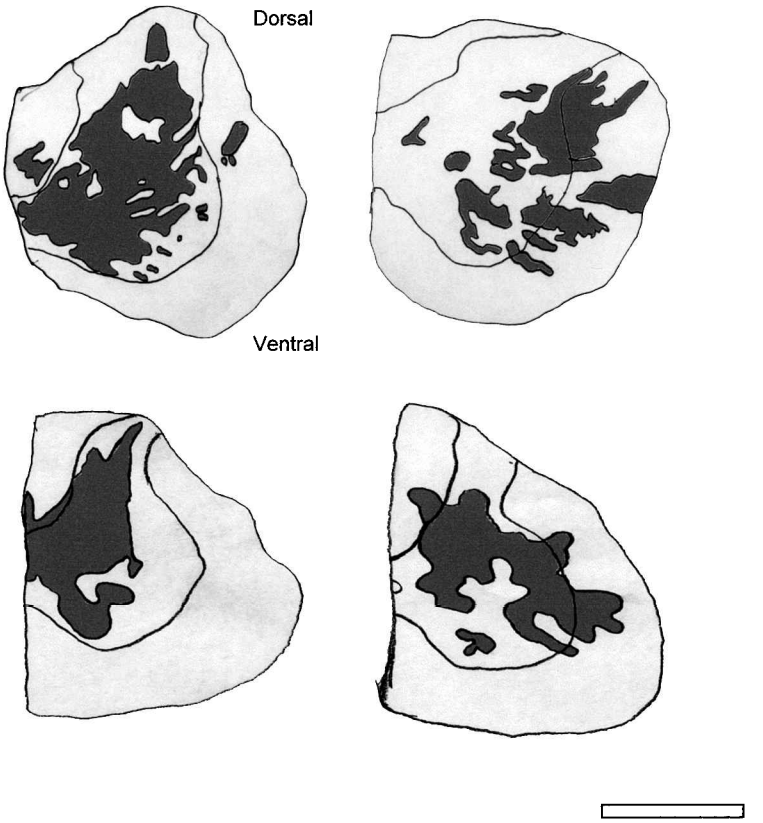

FIG. 1. Camera lucida drawings of spinal cord sections impregnated with rose bengal. Shaded areas indicate the presence of rose bengal spots. Bar = 1000 μm.

(Olympus DP20) attached to the microscope and analyzed using NIH Image software. Spinal cord sections stained GFAP were used for measuring the area of the cystic cavity, because high intensity staining was observed in reactive astrocytes surrounding and delineating the cavity. Several images from a spinal cord section were captured, a photomontage was made using Adobe Photoshop software, and the cross-sectional area of the cavity measured using the NIH Image software. Six to 12 sections from each of the four spinal cord blocks were analyzed. The maximal value of cross-sectional area of cavity was selected as the maximal cord injury induced at each spinal level. Two independent observers made these measurements over the same reconstructed final images, and the final maximum cross-sectional area of cavity by animal and spinal level was the mean value of both observers.

GFAP-immunoreactive cells were counted under the microscope at ×40 magnification using a squared grid in the ocular that covered an area of 0.0625 mm^2. The grid was placed on preserved anterior horns of each spinal cord sections, and all GFAP-labeled cells located within the grid were counted. Only GFAP-immunoreactive cells that showed soma and processes were counted. The density of astrocytes (GFAP-immunoreactive cells/mm^2) was calculated from these counts. If an anterior horn was partially destroyed, the density of astrocytes was calculated in the preserved area. Finally, T9 and L4 CGRP stained spinal cord sections were used for counting the number of CGRP-immunoreactive neurons located in the gray matter of anterior horns.

Statistical Analysis

All histological measurements were performed in a blinded manner. A code of rats and histological slices was used. Data are shown as the mean ± SEM. Statistical comparisons between groups were made by analysis of variance (ANOVA) with a post-hoc Scheffé test for multiple comparisons. Differences were considered significant if $p < 0.05$.

RESULTS

Spinal Cord Infiltration and Structural Changes After Illumination

In RB-bathed spinal cord sections, we observed that the dye easily penetrated the cord parenchyma. Ten min

after cord impregnation, the dye was seen throughout the spinal cord parenchyma, affecting preferentially the gray matter. However, smaller spots in the dorsal and dorsolateral white matter also were seen (Fig. 1).

No apparent gross spinal cord injury was observed in spinal cord sections from rats perfused at 5 and 15-min postirradiation (Fig. 2A). However, in 15-min postirradiation sections, the parenchyma subjacent to dorsal blood vessels was partially disrupted. Blood cells inside the white matter and atrophic or dystrophic myelinated axons were seen in this dorsal area (Fig. 2C). Abnormal myelinated axons were also found in the dorsolateral funiculi (Fig. 2B). Although the blood vessels of the dorsal funiculus were dilated and filled with blood cells, the

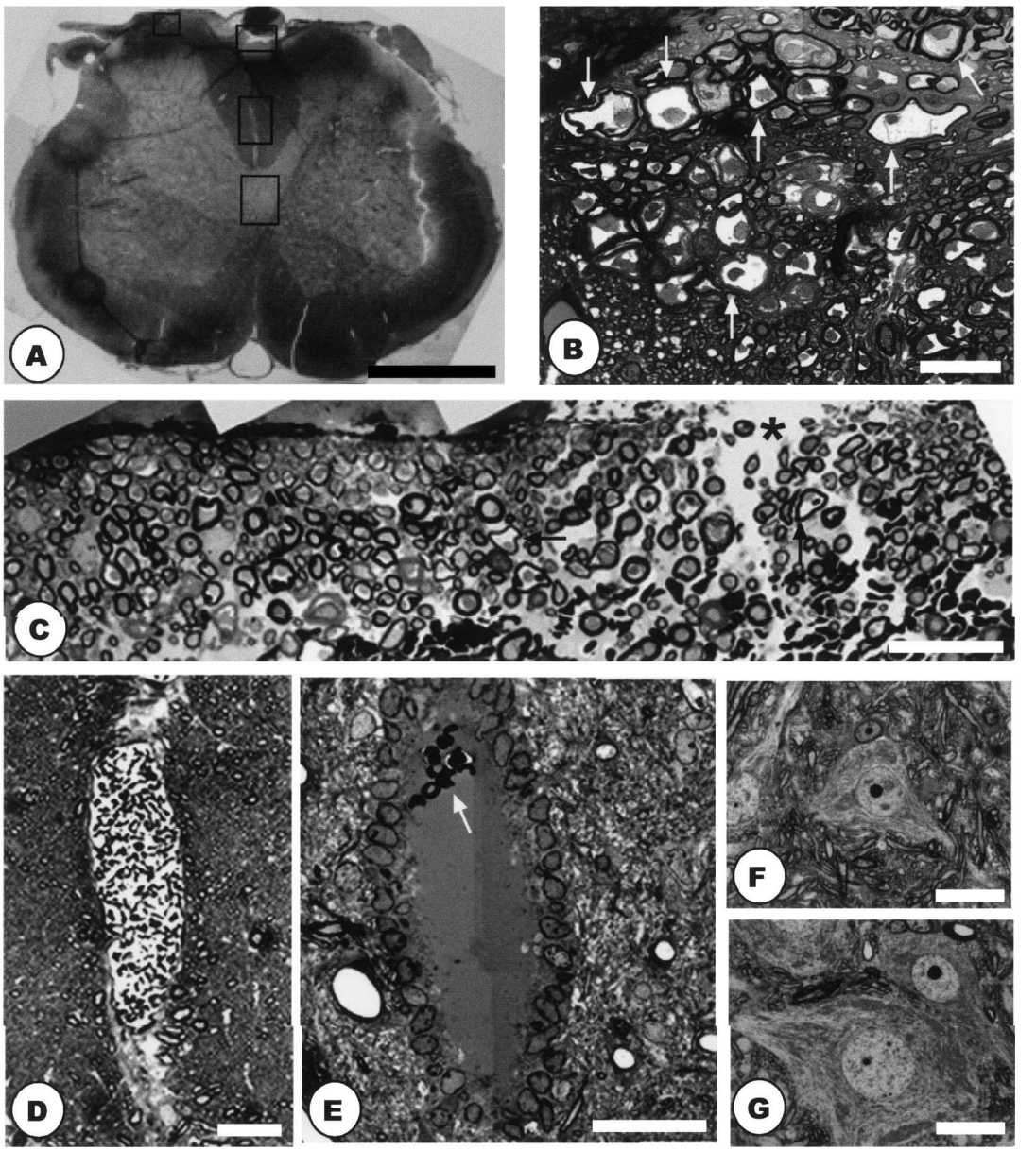

FIG. 2. Photographs at 15 min postillumination. (**A**) Transverse section of the whole spinal cord. (**B**) Image of dystrophic axons located in the left dorsolateral funiculus (arrows). (**C**) Dorsal border subjacent to the blood vessel showing edema (asterisk). Some axons show a dystrophic appearance (arrows). (**D**) Blood vessel filled with blood cells located inside the dorsal funiculus. The surrounded parenchyma has normal appearance. (**E**) Dilated central canal filled with a few erythrocytes (arrow). The neuropil around the central canal looks normal. (**F,G**) Neuronal cells somata located in the ventral gray matter. Bar: A = 1000 μm; B = 20 μm; C = 30 μm; D = 25 μm; E = 30 μm; F,G = 20 μm.

surrounding white matter did not appear damaged (Fig. 2D). The central canal was also dilated and occasionally filled with erythrocytes, but no structural alteration of the surrounding gray matter was seen (Fig. 2E). Neuronal somata of the gray matter had a normal appearance (Fig. 2F,G). In contrast, in animals perfused at 60 min postillumination, marked damage of white matter affecting dorsal and dorsolateral funiculi (Fig. 3A,C), gray com-

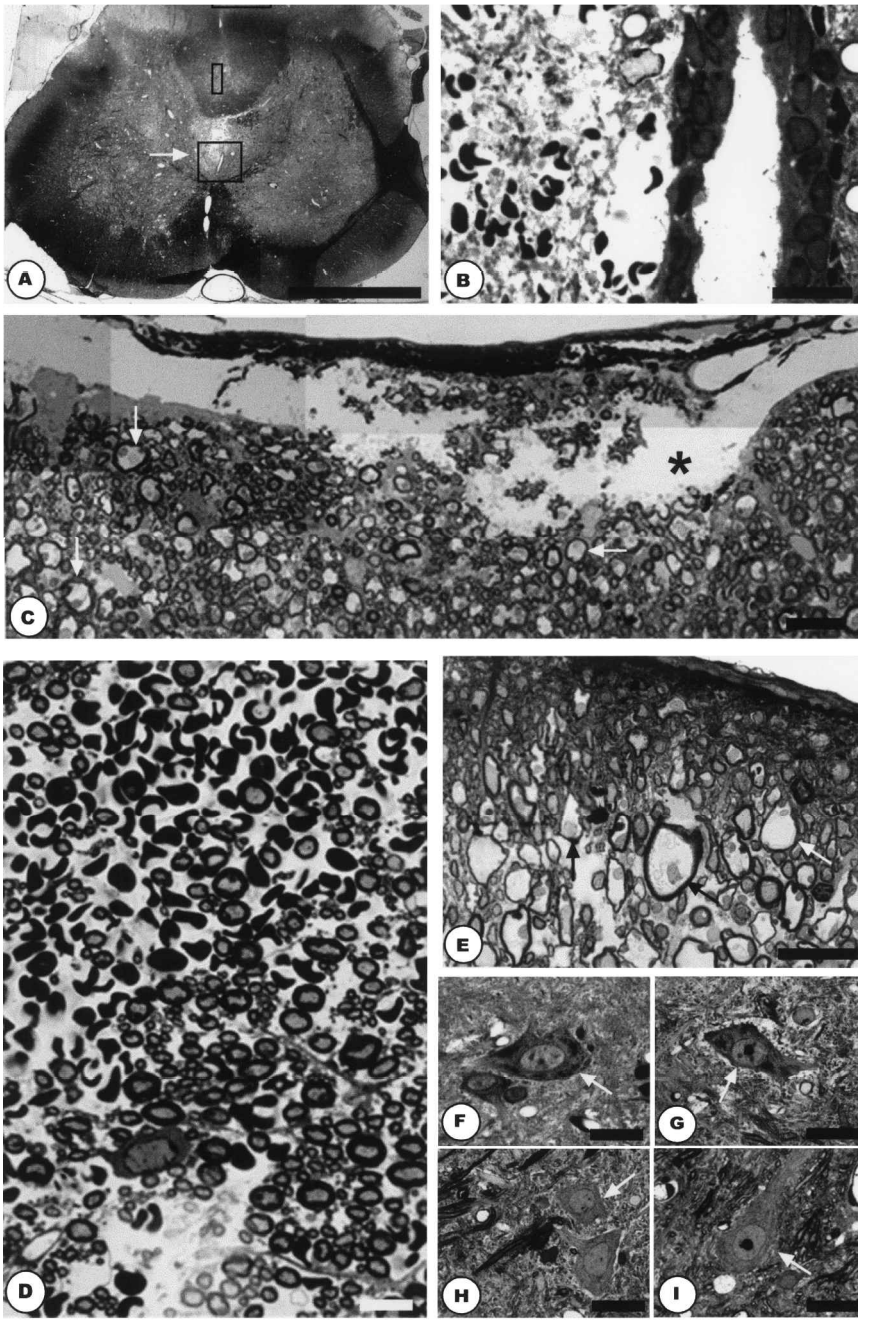

FIG. 3. Photographs at 60 min postillumination. (**A**) Transverse section of the whole spinal cord. The spinal cord parenchyma around the central canal is destroyed (arrow). (**B**) Dilated central canal and hemorrhagic edema in the neuropil around the central canal. (**C**) Dorsal border subjacent to the blood vessel showing edema (asterisk) and dystrophic axons (arrows). (**D**) Hemorrhagic edema affecting the dorsal funiculus, near the corticospinal tract. (**E**) Dystrophic axons located in the left dorsolateral funiculus (arrows). (**F–I**) Somata of neuronal cells in the ventral gray matter (arrows). Dark cells (F,G) are located medially, near disrupted central parenchyma, while light cells (H,I) are located more laterally. Bar: A = 1000 μm; B = 20 μm; C = 25 μm; D = 10 μm; E = 20 μm; F–I = 20 μm.

missural areas near the central canal (Fig. 3A,B) and discrete spots scattered though the nervous parenchyma was observed. Blood cells infiltrating the cord parenchyma were seen in the dorsal funiculus, near the corticospinal tract (Fig. 3D) and around the central canal (Fig. 3B). Dystrophic axons were observed in the dorsolateral funiculi (Fig. 3E). Neuronal somata in the proximity of the damaged areas tended to show a dark cytoplasm (Fig. 3F,G), while those located far from the central areas tended to show a normal appearance (Fig. 3H,I).

Mild and severe effects of injury were observed on the same section. Frequently, only the swelling of astrocytic processes was observed (Fig. 4A,C). In these regions, blood vessels showed a normal structure (Fig. 4C) with normal homotypic endothelial tight junctions, a normal basal lamina and normal endothelial cells and pericytes (Fig. 4C,D). However, in dorsal and dorsolateral funiculi cord regions, a vasogenic edema with erythrocytic extravasation was found (Fig. 4B). Blood vessels, which have not been disrupted, contain erythrocytes, but platelet aggregation was not observed either inside blood vessels nor in the vasogenic edema.

In spinal cord areas with hemorrhagic and/or vasogenic edema, delaminated fibers was observed (Fig. 4B,F). In these areas, oligodendrocytes had a normal appearance, except for altered myelin sheaths (Fig. 4E). In the same myelinated fibers, areas with delamination coexist with areas of normal myelin periodicity. Similar ultrastructural changes affecting myelinated axons in dorsal cord areas were seen in rats perfused at 15 min.

Morphological and Immunohistochemical Results

At T12–L1 spinal cord segments, transverse GFAP-immunostained sections from groups SS10 and RB0 the cord parenchyma showed a normal appearance, with the exception of a very small cavity affecting the dorsal funiculus, subjacent to dorsal blood vessels. In contrast, after 1-min light illumination (group RB1), focal cavities involving the dorsal and dorsolateral funiculi were observed (Fig. 5B). In animals of group RB2.5, spinal cord sections showed a larger cavity affecting the dorsal and dorsolateral funiculi extending to the central canal. Ventral horns, as well as ventrolateral and ventral funiculi remained intact (Fig. 5D). Spinal cord sections from rats of group RB5 showed a larger cystic cavity affecting dorsal and dorsolateral funiculi and the gray matter of dorsal and ventral horns; only the ventrolateral and ventral funiculi appeared preserved (Fig. 5F). With 10 min of illumination (group RB10), most of the spinal cord was destroyed and only a thin rim of tissue remained (Fig. 5H). The maximal area of cystic cavity increased progressively and significantly from SS10 to RB10 groups (Table 1).

Although a lesion was made at T12–L1 segments, the spinal cord injury spread rostrocaudally from the lesion site in all groups. At T9–T10 spinal segments, a small cavity affecting the dorsal funiculus was observed in sections from groups RB1 and RB2.5 rats (Fig. 5A,C), with the mean maximal area of the cavity being 0.08 and 0.10 mm^2, respectively. In animals of group RB5 the cystic cavity averaged 0.35 mm^2, involving dorsal and partially dorsolateral funiculi (Fig. 5E). A larger and open cavity, involving dorsal and dorsolateral funiculi was found in T9–T10 sections from group RB10 (Fig. 5G). A similar pattern was observed caudal to the lesion site at L4–L6 segments.

In spinal cord sections from RB0 and SS10 rats, normal appearing astrocytes with short thin processes showed GFAP but no significant proteoglycan immunostaining, whereas in groups RB1, RB2.5, RB5, and RB10, hypertrophied astrocytes with long and robust processes extending in all directions and heavily immunostained for GFAP and proteoglycan were found (Fig. 6). The density of GFAP-positive astrocytes in preserved gray matter areas was similar in RB1, RB2.5 and RB5 groups at the lesion epicenter (T12–L1). However, an increasing density of GFAP-positive cells was observed between RB1 and RB10 groups at T9–T10 and L4–L6 levels (Table 1). Reactive astroglial hypertrophy matched the severity of the lesion, being slight in sections from group RB1, maximal in RB10 rats, and intermediate in RB2.5 and RB5 rats (Fig. 6). Microglial cells, stained by LEC histochemistry, were present in gray and white matter spinal cord areas of all the animals. In RB0 and SS10 spinal cord sections, ramified LEC-positive cells displayed the typical morphology of resting microglial cells, with an elliptical or elongated cell body and several processes branching out from the perinuclear cytoplasm (Fig. 7A). In lesioned rats, at 15 days most microglial cells had a resting appearance, indistinguishable from those in control rats. However, reactive microglial cells, characterized by short and coarse cell processes and swollen cell bodies, were found in lesioned rats, near the cavity border and also within preserved areas of the spinal cord (Fig. 7B,C). Microglial reactivity ranged from subtle to conspicuous and was more marked in rats with severe injury and in areas close to the lesion epicenter. No amoeboid microglial cells devoid of cell processes and no perivascular infiltrates were found at any location in lesioned rats.

CGRP-immunoreactive fibers were abundant in the dorsal horn gray matter of thoracic and lumbar segments of the spinal cords in groups RB0 and SS10. Labeled afferents entered from the dorsal roots and reached laminae I, II, III, V, and X, and a few arrived to the dorsal gray commissure. At T12–L1 segments of groups RB1

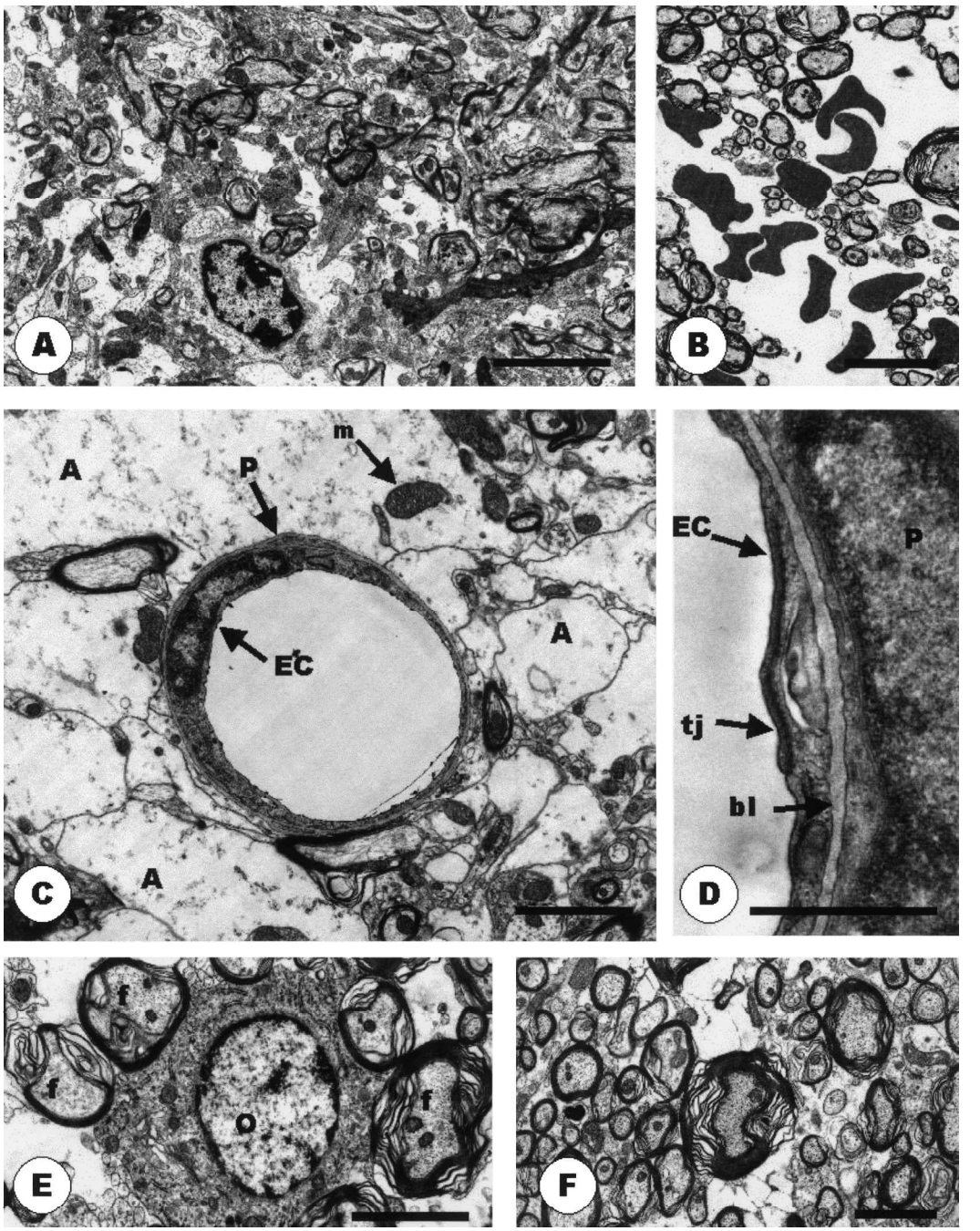

FIG. 4. Electron micrographs from spinal cord postfixed at 60 min postirradiation. (**A**) Cytotoxic edematous small areas in regions showing a low level of severity. Many astrocytic processes are swollen, giving the image of white spots. (**B**) Edema in the dorsolateral funiculus. Myelin delaminations are frequent, and blood cells are present inside the cord parenchyma. (**C**) In spinal cord areas with a higher degree of severity, blood vessels still showed a normal structure. A, swollen astrocytic processes; EC, endothelial cell; P, pericyte; m: mitochondrion. (**D**) High magnification of a capillary wall surrounded by swollen astrocytic feet. EC, endothelial cell; P, pericyte; bl, basal lamina; tj, tight junction. (**E**) At the early acute phase (60 min) delamination is common, but oligodendrocytes may be not affected yet. O, oligodendrocyte; f, myelin fibers. (**F**) Myelin delaminations prior to complete myelin degeneration are first observed in larger fibers. Bar: A,B = 5 μm; C = 2 μm; D = 1 μm; E,F = 2 μm.

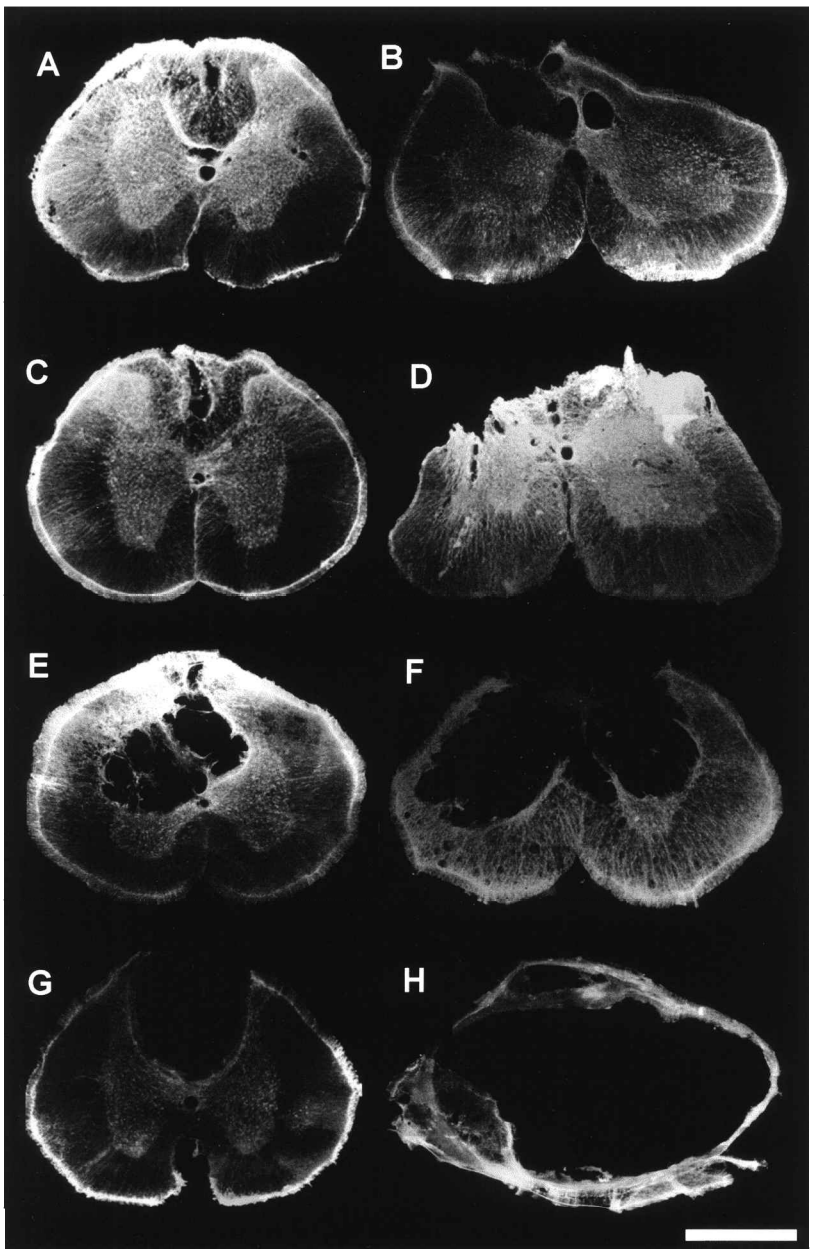

FIG. 5. Spinal cord sections immunostained for GFAP taken at the injured segments T12–L1 (**B,D,F,H**) and at rostral segments T9–T10 (**A,C,E,G**) from RB1 (A,B), RB2.5 (C,D), RB5 (E,F) and RB10 (G,H) rats. Images are representative of the mean changes in each group. Bar = 1000 μm.

to RB10, very faint CGRP-immunoreaction restricted to lamina I was seen in spinal cord sections of lesioned rats, while at T9-T10 and L4-L6 spinal cord levels, where dorsal horns were preserved, afferent CGRP-immunoreactive fibers were observed in laminae I, II and III, and some penetrating up to lamina V. In addition, CGRP-positive neurons, with variable labeling intensity, were located in laminae VIII and IX. These neurons showed a polygonal soma and their staining pattern was in the form of fine punctuated granules filling the perinuclear cytoplasm (Fig. 8). At T9–T10 levels, the number of CGRP-positive somas was similar in spinal cord sections from all experimental groups. However, the number of neurons showing CGRP immunostaining at the L4 level was significantly decreased in RB10 rats with respect to the other experimental groups (Table 1). In spinal cord sec-

Table 1. Histological Results from Spinal Cord Transverse Sections Taken at 15 Days after Photochemical Injury in the Experimental Groups Studied

Parameter	*Segment*	*SS10*	*RB0*	*RB1*	*RB2.5*	*RB5*	*RB10*
Cavity area (mm^2)	T9–T10	0.08 ± 0.03	0.0 ± 0.0	0.08 ± 0.05	0.10 ± 0.02	0.35 ± 0.15	0.40 ± 0.13
	T11	0.02 ± 0.02	0.05 ± 0.03	0.25 ± 0.11	0.38 ± 0.08	0.48 ± 0.15	0.65 ± 0.18
	T12–L1	0.33 ± 0.09	0.32 ± 0.11	0.55 ± 0.06	1.42 ± 0.51	2.68 ± 0.64	5.52 ± 0.83[a,b,c,d,e]
	L2–L3	0.15 ± 0.15	0.07 ± 0.04	0.11 ± 0.05	0.21 ± 0.11	0.47 ± 0.15	4.28 ± 1.73[a,b,c,d,e]
	L4–L6	0.07 ± 0.03	0.0 ± 0.0	0.05 ± 0.03	0.02 ± 0.01	0.15 ± 0.06	0.63 ± 0.23[a,b,c,d,e]
GFAP cells/mm^2	T9–T10	194 ± 31	182 ± 16	264 ± 59	276 ± 53	297 ± 18	489 ± 94[a,b,]
	T11	209 ± 46	200 ± 36	283 ± 33	298 ± 50	307 ± 52	516 ± 29[a,b]
	T12–L1	234 ± 28	221 ± 25	301 ± 22	302 ± 34	308 ± 33	—
	L2–L3	186 ± 35	189 ± 25	274 ± 30	293 ± 59	306 ± 41	568 ± 71[a,b]
	L4–L6	133 ± 41	142 ± 26	237 ± 14	238 ± 52	245 ± 63	478 ± 73[a,b]
CGRP cells	T9	14.2 ± 0.9	14.2 ± 0.4	17.2 ± 1.7	16.3 ± 1.3	17.3 ± 0.9	18.0 ± 1.9
	L4	40.7 ± 0.7	48.3 ± 4.0	40.6 ± 2.6	44.5 ± 4.5	41.6 ± 3.3	5.7 ± 0.8[a,b,c,d,e]

[a]$p < 0.05$ versus SS10; [b]$p < 0.05$ versus RB0; [c]$p < 0.05$ versus RB1; [d]$p < 0.05$ versus RB2.5; [e]$p < 0.05$ versus RB5.

GFAP cells/mm^2: density of GFAP immunolabeled astrocytes per mm^2 in gray matter; CGRP cells, number of CGRP immunolabeled motoneurons in the anterior horn.

tions from RB0 and SS10 rats, CB-positive cells were observed in laminae I, II, and III, and also in the ventral horn lamina IX. A similar pattern was observed in sections from RB1, RB2.5, RB5, and RB10 rats. However, in lesioned groups, CB-positive cells were also seen in laminae VI, VII, VIII, and X (Fig. 8).

DISCUSSION

The present study describes a modified method for photochemical injury and provides evidence that graded histological abnormalities can be produced depending on the time of illumination of the spinal cord. After topical application of RB, irradiation of spinal cord with a fiber-optic light source caused damage to the spinal cord parenchyma. Brain and spinal cord lesions have also been reported after craniotomy or laminectomy, intravenous infusion of RB and illumination with a fiber-optic source (Van Reempts and Borgers, 1994; Van Reempts et al., 1987). However, most studies dealing with photochemical cord injuries have used the method described by Watson et al. (1986), in which RB is administered intravenously and the intact spinal column is irradiated with a 560-nm laser-beam. Laminectomy is not required for inducing the lesion because the translucency of the rat vertebral laminae allows irradiation of the underlying vasculature (Watson et al., 1993). In the present study, a laminectomy was performed because this model was intended for use in transplantation studies (Verdú et al., 2001), in which it would be necessary to access the spinal cord to inject cell suspensions. In previous studies, histopathological examination of 1 min irradiated rats demonstrated a consistent lesion involving the dorsal columns, including corticospinal tracts and dorsolateral funiculi. Necrosis of the dorsal gray horns and areas of intermediate gray matter were also observed while ventral horns were spared. After 5 min irradiation, necrosis involving all white matter tracts except ventrolateral funiculi, and after 10 min, necrosis of the entire cord thickness except for a thin area of white matter located at the ventromedial tracts was seen (Prado et al., 1987). These findings are similar to those described in the present study, where RB was applied topically on the spinal cord dorsal surface and directly irradiated with "cold" light.

Topical application of RB on the peripheral nerve followed by illumination causes acute oxidative damage to peripheral myelin and a subsequent inflammatory response (Van Reempts et al., 1993). A considerable number of axons appeared enlarged, myelin sheaths showed lamellar separation and Schwann cell cytoplasm became intensely vacuolated. In contrast to the observations by Watson et al. (1986), no signs of thrombosis or vascular congestion were detected in the exposed areas of the nerve. The damage observed in peripheral nerve most probably resulted from direct singlet oxygen-induced peroxidation of Schwann cell membranes, including myelin sheaths (Van Reempts et al., 1993). In this study, a similar protocol has been optimized to induce spinal cord lesions of graded severity. RB topically applied on the

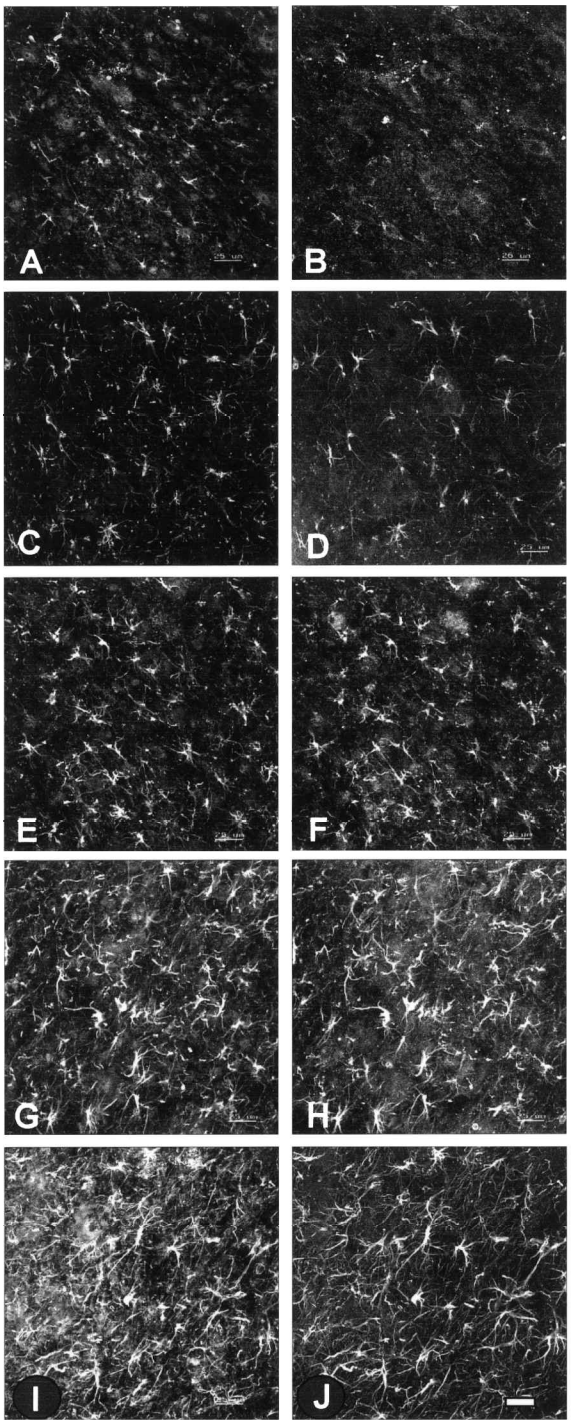

FIG. 6. Confocal images of astrocytes immunolabeled for GFAP (**A,C,E,G,I**) and against 3PE8 (**B,D,F,H,J**) in the gray matter of lumbar cord sections of RB0 (A,B), RB1 (C,D), RB2.5 (E,F), RB5 (G,H) and RB10 (I,J) rats. Images are representative of the mean changes in each group. Bar = 25 μm.

spinal cord easily penetrates the cord parenchyma, from the dorsal surface to ventral gray matter. At 15 and 60 min post-illumination, dystrophic axons and delamination of myelin sheaths were seen in dorsal and dorsolateral funiculi (Figs. 2–4). Areas of disrupted cord parenchyma appeared around the central canal and in the dorsal funiculus, with infiltration of blood cells (see Fig. 3). Electron microscopic examination demonstrated that the endothelial membrane of blood vessels located either near or distant to the most lesioned areas had no particular alterations. However, swollen astrocytic processes were seen surrounding these blood vessels (Fig. 4). Swelling of astrocytic processes around blood vessels in which tight junctions have not been disrupted is a common feature of many pathological states, either ischemic, traumatic, hypoxic or toxic (Bullock et al., 1991; Kimelberg, 1995). During the first 15 days following photochemical injury, damage progresses to form a cystic cavity surrounded by reactive GFAP-immunostained astrocytes. In animals irradiated 1 min, cystic cavities were seen in the dorsal funiculi, suggesting that oligodendrocyte membranes, including their myelin sheaths, were directly affected by the singlet oxygen formed by photosensitized RB. Ultrastructural images demonstrated early myelin involvement. Similar to that observed in the peripheral nerve, infiltration of blood cells was observed in the cord parenchyma, suggesting an inflammatory response to the photochemical illumination.

Our results suggest that reactive RB molecules were produced when illuminated using a light source with a wavelength in the visible spectrum. The calorific energy only slightly increases the RB effects. RB is a classic singlet oxygen generator when illuminated (Lamberts and Neckers, 1985). Two major photochemical reaction models are possible. In type I reactions, an electron or a hydrogen atom is transferred between the light-excited sensitized and the substrate to give free radical forms of the molecules. These can then undergo various types of reactions to give oxidized products of the substrate and, in most cases, regeneration of unexcited sensitized molecules. Reactive oxygen species that can damage biological systems, including superoxide, hydrogen peroxide and hydroxyl radicals, are often formed. In type II reactions, excitation energy is transferred from triplet sensitizer to ground state oxygen molecules, giving ground state sensitizer and a singlet state of oxygen. Singlet oxygen rapidly reacts with electrophilic biomolecules such as unsaturated lipids, proteins and nucleic acids. Often, type I and II reactions occur simultaneously in competition (Spikes, 1991). Diluted in saline solution, the quantum yield of singlet oxygen production by RB is 0.75, whereas other xanthene dyes such as fluorescein or eosin Y pro-

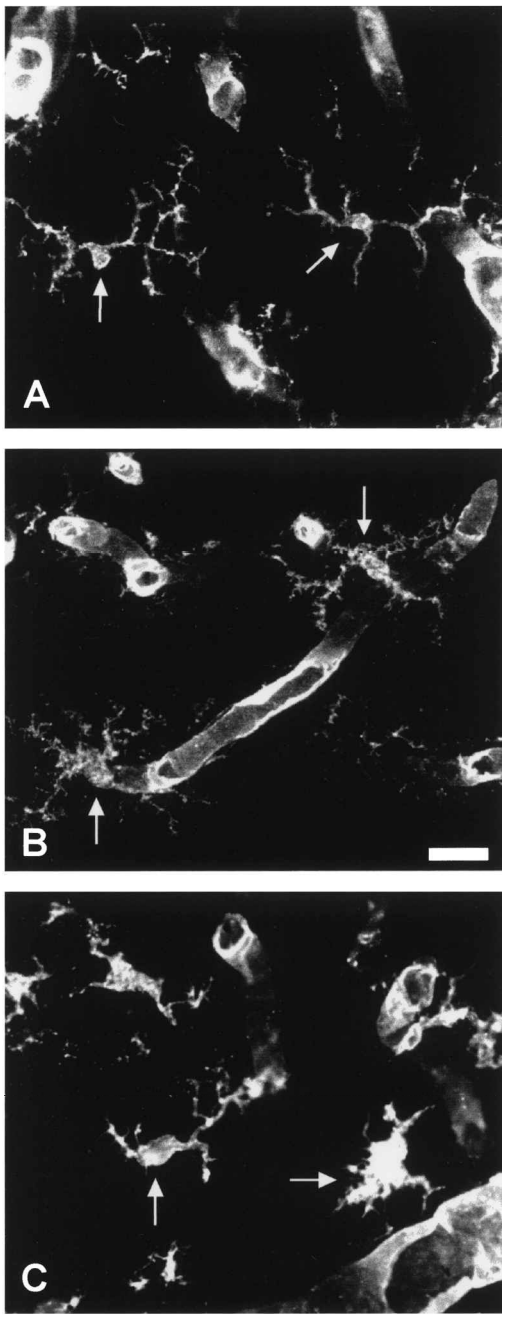

FIG. 7. Images of microglial cells stained with tomato lectin (arrows) in gray matter in the L4–L6 segment of RB0 (**A**), RB2.5 (**B**), and RB10 (**C**) rats. Bar = 10 μm.

duce lower quantities (Spikes, 1991). Peroxidative damage to the endothelial membrane provides the initial stimulus for platelet adhesion and eventual thrombus formation, which explain brain and spinal cord infarction when RB is injected intravenously. However, direct peroxidation of glial membranes by singlet oxygen molecules may most likely explain the effects observed when RB is applied topically on peripheral and central nerve tissue, as we did not observe blood vessel occlusion or thrombosis.

Another source of free radicals is the glutamate neurotoxicity that appears after injury. After spinal cord injury glutamate levels increase about 10-fold during the first 30 min (Liu et al., 1991; Mills et al., 2001). Concentrations are maximal at the injury epicenter and decrease becoming undetectable beyond 5 mm from the injury epicenter (McAddo et al., 1999). During this early phase toxicity is caused by glutamate binding to its receptors. The first component of glutamate toxicity, marked by acute neuronal swelling, depends on the uptake of extracellular Na^+ and Cl^- by the cell that causes plasma membrane depolarization. Depolarization causes Ca^{2+} channel opening and massive influx of Ca^{2+} that initiates a cascade-like effect leading to cell death. Ca^{2+} influx converts xanthine dehydrogenase into xanthine oxidase thus allowing for superoxide anion and hydrogen peroxide (Atlante et al., 2001; Lewén et al., 2000). Under normal conditions, glutamate is removed from the extracellular space because glutamate transporters are found on neurons as well as astroglial cells. However, after central nervous system injury the reactive oxygen species generated at the lesion site inhibit glutamate uptake by oxidation of glutamate transporters (Danbolt, 2001). Recently, Ogita et al. (2001) reported that rose bengal inhibits glutamate uptake into synaptic vesicles. In addition, Kim et al (2001) reported that singlet oxygen derived from photoactivated dyes (methylene blue and rose bengal) is capable of damaging superoxide dismutase and catalase, two antioxidant enzymes. In summary, photoactivated rose bengal directly promotes the formation of reactive oxygen species and inhibits the biological defense systems against them, and indirectly also raises reactive oxygen species production by inhibiting glutamate uptake.

In spinal cord sections from RB1, RB2.5, RB5, and RB10 rats we found a graded increase in intensity of GFAP and proteoglycan (3PE8) immunoreactivity at 15 days. The counts of GFAP-immunoreactive cells were slightly lower in distal levels than at the lesion site. After contusion injuries of varying loads to the exposed rat spinal cord a progressive increase of GFAP immunoreactivity has been described in relation to the load and to the functional deficit induced (Farooque et al., 1995); increased expression of GFAP was present already 4 h after injury. After hemisection (Leme and Chadi, 2001), moderate contusion (Baldwin et al., 1998) and photochemical injury (Koshinaga et al., 1993), increased GFAP immunoreactivity was seen in spinal cord regions close to the wound and tended to decrease distally to the lesion site. Chondroitin sulfate proteoglycan (CSPG) im-

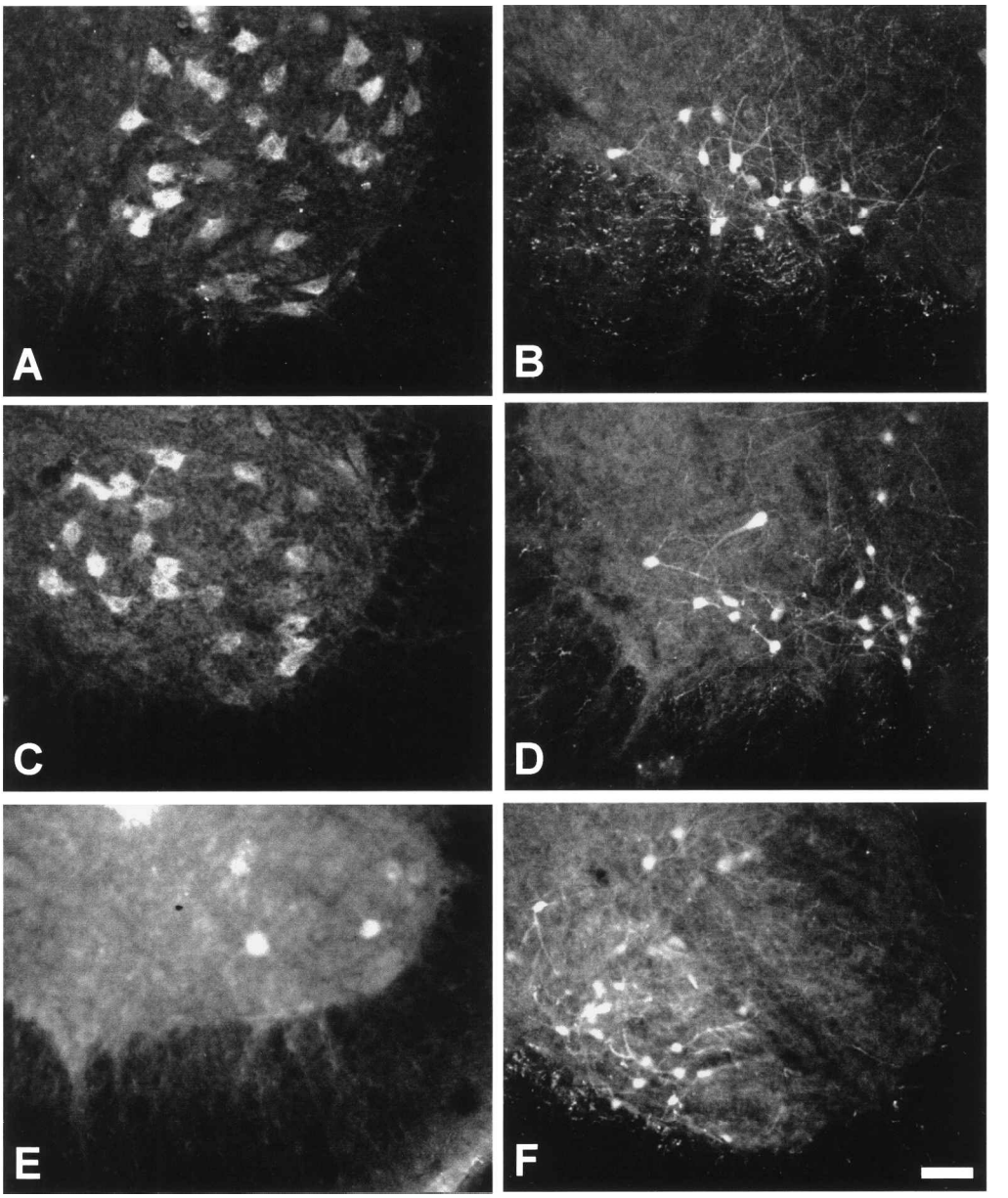

FIG. 8. Images of ventral horns immunolabeled against CGRP (**A,C,E**) and against calbindin (**B,D,F**) of RB0 (A,B), RB2.5 (C,D), and RB10 (E,F) experimental groups at L4–L6 level. Bar = 100 μm.

munoreactivity increases also after injury expressed by reactive astrocytes. Recently, Plant et al. (2001) reported that CSPGs immunoreactivity was greater at the caudal Schwann cell graft–host cord interface than at the rostral interface, and it was associated with astrocytes and fibroblasts. We observed hypertrophied GFAP- and proteoglycan-immunoreactive cells in spinal cord sections even several segments distal to the lesion epicenter. In vitro studies demonstrated that proteoglycan inhibits neurite outgrowth, and that a monoclonal antibody against proteoglycan neutralized this inhibitory activity (Bovolenta et al., 1997). These findings suggest that accumulation of proteoglycan compounds near the wound and in more distal spinal cord regions may impair the elongation of injured central axons. In fact, chondroitinase–ABC treatment, which degrades CSPGs, allows neurite elongation (Zuo et al., 1998) and promotes axonal regeneration after spinal cord injury (Bradbury et al., 2002; Yick et al., 2000).

After contusion and photochemical injury to the spinal

cord, accumulation of phagocytic amoeboid microglia/macrophages occur during the first week postlesion but by the second week only process-bearing microglia were found (Koshinaga and Whittemore, 1995; Popovich and Hickey, 2001; Schnell et al., 1999). These findings are in agreement with our observations that reactive ramified microglia but no amoeboid cells were found at 15 days postlesion. The presence of microglial cells showing morphological signs of reactivity at this late phase is consistent with the finding that lesion-induced inflammatory responses are significantly higher, more widespread and persist for a longer period in the spinal cord than in the brain (Schnell et al., 1999). It is known that delayed apoptotic neuronal and glial cell death in the spinal cord still occurs 14 days after contusion (Yong et al., 1998), and it may provide the stimulus for persistent microglial activation. We also found that microglial reactivity after photochemical injury was more evident with increasing severity of the lesion, similar to findings after contusion (Carlson et al., 1998), photochemical (Koshinaga and Whittemore, 1995) or hemisection (Leme and Chadi, 2001) injuries in the spinal cord.

After a complete spinal cord transection the expression of CGRP decreases in motoneurons caudal and increases in motoneurons rostral to the transection, although the number of neurons expressing CGRP does not differ from controls (Arvidsson et al., 1993; Krenz and Weaver, 1996; Marlier et al., 1990). However, selective destruction of serotoninergic and noradrenergic supraspinal inputs results in increased levels of CGRP and its mRNA in motoneurons below the lesion (Arvidsson et al., 1993). In the present study we observed only a significant decrease of the number of CGRP-positive lumbar motoneurons in spinal cord sections from RB10 rats, in which the spinal cord was completely injured at T12–L1. In lumbar cord sections of RB10 rats motoneurons were strongly labeled against CGRP, while in groups RB1, RB2.5, and RB5, with total or partial preservation of descending pathways, lumbar motoneurons were more heterogeneously stained against CGRP (Fig. 8). Supraspinal afferents, preferentially brainstem descending pathways, seem to have a strong influence on motoneurons, and CGRP, acetylcholine (Brambilla et al., 1996) and other neuronal markers expression is related to the functional state and type of inputs of the motoneurons.

In non-lesioned spinal cords, we found medium to large size CB-positive neurons in laminae VII and IX (Arvidsson et al., 1992; Ren and Ruda, 1994). The CB-immunostained neurons located at lamina IX have been identified as Renshaw cells (Arvidsson et al., 1992; Carr et al., 1998). In various animals models of neurodegenerative diseases, Iacopino et al. (1992) reported that CB-containing neurons remained after exposure to neurotoxins, while other neurons were lost, suggesting that the presence of calbindin may protect neurons from calcium-mediated neurotoxicity. In the present work we observed CB-immunostained neurons in ventral horns of both control and lesioned rats. However, lesioned rats also showed CB-positive neurons in central areas (laminae VI–VIII) of spinal cord segments rostral and caudal to the lesion, suggesting that neuronal expression of calbindin may be related to protection of spinal neurons. In this context, expression of calbindin in motoneuron cells after retroviral infection with calbindin cDNA prevents amyotrophic lateral sclerosis IgG-mediated cytotoxicity, while treatment with calbindin antisense oligodeoxynucleotides rendered these cells vulnerable again to IgG toxicity (Ho et al., 1996).

In summary, the present study shows that graded spinal cord injuries can be induced by a photochemical lesion induced in adult rats by topical application of RB and illumination with a light source. Our results demonstrate that, by increasing the illumination time, morphological consequences are progressively more severe. This experimental model therefore may be adequate for investigating different therapeutic strategies. Using the described method of lesion we recently studied the influence of olfactory ensheathing cells transplanted into the damaged spinal cord, and found that they exert a neuroprotective role by reducing astrocytic gliosis and cystic cavitation (Verdú et al., 2001).

ACKNOWLEDGMENTS

We thank Dr. Manuel Nieto-Sampedro and Vilma C. Muñetón from the Instituto Cajal (CSIC, Madrid, Spain) for supplying monoclonal antibodies against proteoglycan. Thanks are also given to Dr. Mercè Martí and Onofre Castell from the Servei de Microscòpia (UAB), and Josep Graells, Albert Brillas, and Mónica Espejo for technical assistance. This research was supported by grants from the Ministerio de Sanidad y Consumo (FISss 00/0031-02), Societat Catalana de Neurologia-Fundació Uriach, and Sociedad Española de Neurología, Spain.

REFERENCES

ACARIN, L., VELA, J.M., GONZÁLEZ, B., et al. (1994). Demonstration of poly-*N*-acetyl lactosamine residues in ameboid and ramified microglial cells in rat brain by tomato lectin binding. J. Histochem. Cytochem. **42,** 1033–1041.

ANDERSON, T.E., and STOKES, B.T. (1992). Experimental models for spinal cord injury research: physical and physiological considerations. J. Neurotrauma **9,** S135–S142.

ARVIDSSON, U., CULLHEIM, S., ULFHAKE, B., et al.

(1989). Altered levels of calcitonin gene-related peptide (CGRP)-like immunoreactivity of cat lumbar motoneurons after chronic spinal cord transection. Brain Res. **489,** 387–391.

ARVIDSSON, U., PIEHL, F., JOHNSON, H., et al. (1993). The peptidergic motoneurone. Neuroreport **4,** 849–856.

ARVIDSSON, U., ULFHAKE, B., CULLHEIM, S., et al. (1992). Distribution of calbindin D28k-like immunoreactivity (LI) in the monkey ventral horn: do Renshaw cells contain calbindin D28k-LI? J. Neurosci. **12,** 718–728.

ATLANTE, A., CALISSANO, P., BOBBA, A., et al. (2001). Glutamate neurotoxicity, oxidative stress and mitochondria. FEBS Lett. **497,** 1–5.

BALDWIN, S.A., BRODERICK, R., BLADES, D.A., et al. (1998). Alterations in temporal/spatial distribution of GFAP- and vimentin-positive astrocytes after spinal cord contusion with the New York University spinal cord injury device. J. Neurotrauma **15,** 1015–1026.

BEATTIE, M.S., FAROOQUI, A.A., and BRESNAHAN J.C. (2000). Review of current evidence for apoptosis after spinal cord injury. J. Neurotrauma **17,** 915–925.

BLESCH, A., and TUSZYNSKI, M.H. (2001). GDNF gene delivery to injured adult CNS motor neurons promotes axonal growth, expression of the trophic neuropeptide CGRP, and cellular protection. J. Comp. Neurol. **436,** 399–410.

BORKE, R.C., CURTIS, M., and GINSBERG, C. (1993). Choline acetyltransferase and calcitonin gene-related peptide immunoreactivity in motoneurons after different types of nerve injury. J. Neurocytol. **22,** 141–153.

BOVOLENTA, P., FERNAUD-ESPINOSA, I., MÉNDEZ-OTERO, R., et al. (1997). Neurite outgrowth inhibitor of gliotic brain tissue. Mode of action and cellular localization, studied with specific monoclonal antibodies. Eur. J. Neurosci. **9,** 977–989.

BRADBURY, E.J., MOON, L.D.F., POPAT, R.J., et al. (2002). Chondroitinase ABC promotes functional recovery after spinal cord injury. Nature **416,** 636–640.

BRAMBILLA, G., SANGIOVANNI, G., PUGLIESE, R., et al. (1996). Alteration of complex IV and acetylcholine-related enzymes in experimental spinal cord injury. J. Neurosurg. Sci. **40,** 213–219.

BULLOCK, R., MAXWELL, W.L., GRAHAM, D.I., et al. (1991). Glial swelling following human cerebral contusion: an ultrastructural study. J Neurol. Neurosurg. Psychiatry **54,** 427–434.

BUNGE, M.B., HOLETS, V.R., BATES, M.L., et al. (1994). Characterization of photochemically induced spinal cord injury in the rat by light and electron microscopy. Exp. Neurol. **127,** 76–93.

CALDERÓ, J., CASANOVAS, A., SORRIBAS, A., et al. (1992). Calcitonin gene–related peptide in rat spinal cord motoneurons: subcellular distribution and changes induced by axotomy. Neuroscience **48,** 449–461.

CAMERON, T., PRADO, R., WATSON, B.D., et al. (1990). Photochemically induced cystic lesion in the rat spinal cord. I. Behavioral and morphological analysis. Exp. Neurol. **109,** 214–223.

CARLSON, S.L., PARRISH, M.E., SPRINGER, J.E., et al. (1998). Acute inflammatory response in spinal cord following impact injury. Exp. Neurol. **151,** 77–88.

CARR, P.A., ALVAREZ, F.J., LEMAN, E.A., et al. (1998). Calbindin D28k expression in immunohistochemically identified Renshaw cells. Neuroreport **9,** 2657–2661.

DANBOLT, N.C. (2001). Glutamate uptake. Prog. Neurobiol. **65,** 1–105.

FAROOQUE, M., BADONIC, T., OLSSON, Y., et al. (1995). Astrocytic reaction after graded spinal cord compression in rats: immunohistochemical studies on glial fibrillary acidic protein and vimentin. J. Neurotrauma **12,** 41–52.

GIBSON, S.J., POLAK, J.M., BLOOM, S.R., et al. (1984). Calcitonin gene–related peptide immunoreactivity in the spinal cord of man and of eight other species. J. Neurosci. **4,** 3101–3011.

HO, B.K., ALEXIANU, M.E., COLOM, L.V., et al. (1996). Expression of calbindin-D28k in motoneuron hybrid cells after retroviral infection with calbindin-D28k cDNA prevents amyotrophic lateral sclerosis IgG-mediated cytotoxicity. Proc. Natl. Acad. Sci. USA **93,** 6796–6801.

IACOPINO, A., CHRISTAKOS, S., GERMAN, D., et al. (1992). Calbindin-D28k-containing neurons in animal models of neurodegeneration: possible protection from excitotoxicity. Brain Res. Mol. Brain Res. **13,** 251–261.

KIM, S. Y., KWON, O.J., and PARK, J.W. (2001). Inactivation of catalase and superoxide dismutase by singlet oxygen derived from photoactivated dye. Biochimie **83,** 437–444.

KIMELBERG, H.K. (1995). Brain edema, in: *Neuroglia.* H. Kettenman, and B.R. Ramson (eds), Oxford University Press: New York, pps. 919–935.

KÖBBERT, C., and THANOS, S. (2000). Topographic representation of the sciatic nerve motor neurons in the spinal cord of the adult rat correlates to region-specific activation patterns of microglia. J. Neurocytol. **29,** 271–283.

KOSHINAGA, M., and WHITTERMORE, S.R. (1995). The temporal and spatial activation of microglia in fiber tracts undergoing anterograde and retrograde degeneration following spinal cord lesion. J. Neurotrauma **12,** 209–222.

KOSHINAGA, M., SANON, H.R., and WHITTERMORE, S.R. (1993). Altered acidic and basic fibroblast growth factor expression following spinal cord injury. Exp. Neurol. **120,** 32–48.

KRENZ, N.R., and WEAVER, L.C. (1996). CGRP expression increases in the ventral horn rostral to spinal cord transection. Neuroreport **25,** 2859–2862.

KRENZ, N.R., and WEAVER, L.C. (2000). Nerve growth factor in glia and inflammatory cells of the injured rat spinal cord. J. Neurochem. **74,** 730–739.

KREUTZBERG, G.W. (1996). Microglia: a sensor for pathological events in the CNS. Trends Neurosci. **19,** 312–318.

LAMBERTS, J.J.M., and NECKERS, D,C. (1985). Rose bengal derivates as singlet oxygen sensitizers. Tetrahedron **41,** 2183–2190.

LEME, R.J., and CHADI, G. (2001). Distant microglial and astroglial activation secondary to experimental spinal cord lesion. Arq. Neuropsiquiatr. **59,** 483–492.

LEMONS, M.L., HOWLAND, D.R., and ANDERSON, D.K. (1999). Chondroitin sulfate proteoglycan immunoreactivity increases following spinal cord injury and transplantation. Exp. Neurol. **160,** 51–65.

LEWÉN, A., MATZ, P., and CHAN, P.H. (2000). Free radical pathways in CNS injury. J. Neurotrauma **17,** 871–890.

LIU, D., THANGNIPON, W., and McADOO, D.J. (1991). Excitatory amino acids rise to toxic levels upon impact injury to the rat spinal cord. Brain Res. **547,** 344–348.

MARLIER, L., RAJAOFETRA, N., PERETTI-RENUCCI, R., et al. (1990). Calcitonin gene-related peptide staining intensity is reduced in rat lumbar motoneurons after spinal cord transection: a quantitative immunocytochemical study. Exp. Brain Res. **82,** 40–47.

McADOO, D.J., XU, G.Y., ROBAK, G., et al. (1999). Changes in amino acid concentrations over time and space around an impact injury and their diffusion through the rat spinal cord. Exp. Neurol. **159,** 538–544.

MELINEK, R., HOLETS, V.R., PUCKETT, W.R., et al. (1994). Calcitonin gene-related peptide (CGRP)–like immunoreactivity in motoneurons of the human spinal cord following injury. J. Neurotrauma **11,** 63–71.

MILLS, C.D., XU, G.Y., McADOO, D.J., et al. (2001). Involvement of metabotropic glutamate receptors in excitatory amino acid and GABA release following spinal cord injury in rat. J. Neurochem. **79,** 835–848.

NAVARRO, X., BUTÍ, M., and VERDÚ, E. (1994). Autotomy prevention by amitriptyline after peripheral nerve section in different strains of mice. Restor. Neurol. Neurosci. **6,** 151–157.

NICOTERA, P., BELLOMO, G., and ORRENIUS, S. (1992). Calcium-mediated mechanisms in chemically induced cell death. Annu. Rev. Pharmacol. Toxicol. **32,** 449–470.

OGITA, K., HIRATA, K., BOLE, D.G., et al. (2001). Inhibition of vesicular glutamate storage and exocytotic release by rose bengal. J. Neurochemistry **77,** 34–42.

PLANT, G.W., BATES, M.L., and BUNGE, M.B. (2001). Inhibitory proteoglycan immunoreactivity is higher at the caudal than the rostral Schwann cell graft-transected spinal cord interfaces. Mol. Cell Neurosci. **17,** 471–487.

POPOVICH, P.G., and HICKEY, W.F. (2001). Bone marrow chimeric rats reveal the unique distribution of resident and recruited macrophages in the contused rat spinal cord. J. Neuropathol. Exp. Neurol. **60,** 676–685.

PRADO, R., DIETRICH, W.D., WATSON, B.D., et al. (1987). Photochemically induced graded spinal cord infaction. Behavioral, electrophysiological and morphological correlates. J. Neurosurg. **67,** 745–753.

REN, K., and RUDA, M.A. (1994). A comparative study of the calcium-binding proteins calbindin-D28k, calretinin, calmodulin and parvalbumin in the rat spinal cord. Brain Res. Rev. **19,** 163–179.

SCHNELL, L., FEARN, S., KLASSEN, H., et al. (1999). Acute inflammatory responses to mechanical lesions in the CNS: differences between brain and spinal cord. Eur. J. Neurosci. **11,** 3648–3658.

SPIKES, J.D. (1991). Applications of dye-sensitized photoreactions in neurobiology. Photochem. Photobiol. **54,** 1079–1092.

VAN REEMPTS, J., and BORGERS, M. (1994). Histopathological characterization of photochemical damage in nervous tissue. Histol. Histopathol. **9,** 185–195.

VAN REEMPTS, J., VAN DEUREN, B., ASHTON, D., et al. (1993). A new model of photochemically induced acute and reversible demyelination in the peripheral nervous system. Exp. Neurol. **120,** 283–290.

VAN REEMPTS, J., VAN DEUREN, B., VAN DE VEN, M., et al. (1987). Flunarizine reduces cerebral infarct size after photochemically induced thrombosis in spontaneously hypertensive rats. Stroke **18,** 1113–1119.

VERDÚ, E., GARCÍA-ALÍAS, G., FORÉS, J., et al. (2001). Effects of ensheathing cells transplanted into photochemically damaged spinal cord. Neuroreport **12,** 2303–2309.

VON EULER, M., SUNDSTRÖM, E., and SEIGER, A. (1997). Morphological characterization of the envolving rat spinal cord injury after photochemically induced ischemia. Acta Neuropathol. **94,** 232–239.

WATSON, B.D., HOLETS, V.R., PRADO, R., et al. (1993). Laser-driven photochemical induction of spinal cord injury in the rat: methodology, histopathology and applications. Neuroprotocols **3,** 3–15.

WATSON, B.D., PRADO, R., DIETRICH, W.D., et al. (1986). Photochemically induced spinal cord injury in the rat. Brain Res. **367,** 296–300.

WRATHALL, J.R. (1992). Spinal cord injury models. J. Neurotrauma **9,** S129–S134.

YICK, L.W., WU, W., SO, K.F., et al. (2000). Chondroitinase ABC promotes axonal regeneration of Clarke's neurons after spinal cord injury. Neuroreport **11,** 1063–1067.

YONG, C., ARNOLD, P.M., ZOUBINE, M.N., et al. (1998). Apoptosis in cellular compartments of rat spinal cord after severe contusion injury. J. Neurotrauma **15,** 459–472.

ZUO, J., NEUBAUER, D., DYESS, K., et al. (1998). Degradation of chondroitin sulfate proteoglycan enhances the neurite-promoting potential of spinal cord tissue. Exp. Neurol. **154,** 654–662.

Address reprint requests to:
Enrique Verdú, Ph.D.
Departament de Biologia Cellular
Fisiologia i Immunologia
Unitat de Fisiologia Mèdica
Edif. M
Universitat Autònoma de Barcelona
E-08193 Bellaterra, Spain

E-mail: Enric.Verdu@uab.es